

UNPUBLISHED PRELIMINARY DATA

R-104 - 217
Task #1

ORNL-3722
UC-34 - Physics
TID-4500 (36th ed.)

THE SPACE, TIME, AND ENERGY DISTRIBUTIONS OF
THE PROTON BEAM OF THE HARVARD UNIVERSITY
SYNCHROCYCLOTRON

R. T. Santoro

FACILITY FORM 608

N 65 16340
(ACCESSION NUMBER)

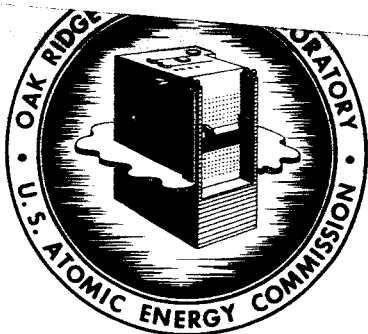
33
(PAGES)

CR 60600
(INASA CR OR TMX OR AD NUMBER)

(THRU)

(CODE)

(CATEGORY)



OAK RIDGE NATIONAL LABORATORY

operated by

UNION CARBIDE CORPORATION

for the

U.S. ATOMIC ENERGY COMMISSION

GPO PRICE \$ _____

OTS PRICE(S) \$ _____

Hard copy (HC) 2.00

Microfiche (MF) .50

Printed in USA. Price \$2.00. Available from the Clearinghouse for Federal
Scientific and Technical Information, National Bureau of Standards,
U.S. Department of Commerce, Springfield, Virginia

LEGAL NOTICE

This report was prepared as an account of Government sponsored work. Neither the United States, nor the Commission, nor any person acting on behalf of the Commission:

- A. Makes any warranty or representation, expressed or implied, with respect to the accuracy, completeness, or usefulness of the information contained in this report, or that the use of any information, apparatus, method, or process disclosed in this report may not infringe privately owned rights; or
- B. Assumes any liabilities with respect to the use of, or for damages resulting from the use of any information, apparatus, method, or process disclosed in this report.

As used in the above, "person acting on behalf of the Commission" includes any employee or contractor of the Commission, or employee of such contractor, to the extent that such employee or contractor of the Commission, or employee of such contractor prepares, disseminates, or provides access to, any information pursuant to his employment or contract with the Commission, or his employment with such contractor.

CASE FILE COPY

Contract No. W-7405-eng-26

Neutron Physics Division

THE SPACE, TIME, AND ENERGY DISTRIBUTIONS OF THE PROTON BEAM
OF THE HARVARD UNIVERSITY SYNCHROCYCLOTRON*

Report Written by

R. T. Santoro

Work Performed by

W. R. Burrus, W. A. Gibson, N. W. Hill,**
C. F. Johnson (General Dynamics), T. A. Love,
F. C. Maienschein, R. W. Peelle, R. T. Santoro,
J. W. Wachter, W. Zobel

JANUARY 1965

OAK RIDGE NATIONAL LABORATORY
Oak Ridge, Tennessee
operated by
UNION CARBIDE CORPORATION
for the
U.S. ATOMIC ENERGY COMMISSION

*Work supported by the National Aeronautics and Space Administration under
NASA Order R-104.

**Instrumentation and Controls Division.

CONTENTS

	Page
Abstract.....	1
Introduction.....	3
Beam Distribution in Space.....	3
Calculation of the Proton Distribution.....	5
Experimental Results.....	8
Beam Location Stability.....	12
Distribution in Time.....	15
Measurement of the Macrostructure.....	15
Measurement of the Microstructure.....	17
Proton Energy Distribution.....	18
Beam Energy from Proton Range in Copper.....	20
Conclusions to the Proton Beam Measurements.....	27
Acknowledgements.....	30

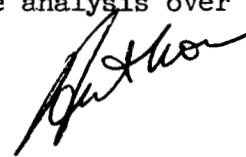
THE SPACE, TIME, AND ENERGY DISTRIBUTIONS OF THE PROTON BEAM
OF THE HARVARD UNIVERSITY SYNCHROCYCLOTRON

ABSTRACT

16340

The space, time, and energy distributions of the proton beam of the Harvard University Synchrocyclotron were measured. The spatial distribution was estimated from multiple-scattering approximations and measured by means of x-ray films and a beam profile counter telescope. Experimental results may be approximated by a Gaussian function with $\sigma = \pm 0.28$ cm, with agreement between the observed results and the multiple-scattering estimates being favorable. Ninety-eight percent of the protons were contained in an 0.84-cm beam radius. Analysis of the macroburst structure revealed a gross duty cycle of $(4 \pm 2)\%$, depending upon proton injection and extraction parameters. Oscilloscope observations of the microstructure showed that the protons occurred at regular 42-nsec intervals, with the width of the time distribution of protons being less than 7 nsec. With the delayed coincidence technique, the standard deviation of the time between adjacent bursts of protons was 1.4 nsec.

The proton beam energy was determined from measurements of the proton range in copper and from time-of-flight measurements. The beam energy determined from the range measurements was 160.3 ± 0.6 MeV. The rms range spread was measured from the differential range curve as 0.34 ± 0.05 g/cm², compared with the calculated straggling standard deviation of 0.32 g/cm². The proton energy measured by flight-time analysis over a 355-cm flight path was 153.38 ± 4.1 MeV.



INTRODUCTION

Experiments performed at the Harvard University Synchrocyclotron^{1,2} to determine the energy spectra at various angles for secondary neutrons, protons, and gamma rays required that the space, time, and energy distributions of the proton beam be well known. Knowledge of these parameters was necessary for the design of experimental instrumentation and for the analysis of the spectral data.

The synchrocyclotron (shown in Fig. 1) is shielded by concrete 3 to 8 ft thick and is a frequency-modulated machine capable of producing unpolarized 160(+2%)-MeV protons at rates as high as 5×10^{10} protons/sec. Modulation is achieved with a rotating 16-tooth condenser through a frequency range of 23 to 30 Mc/sec.

Following extraction, the beam is passed through three sets of collimating slits, a steering magnet, and finally a quadrupole magnet. Beam location is controlled by the steering magnet, and focusing is achieved by optimizing the slit openings and the quadrupole magnet current.

BEAM DISTRIBUTION IN SPACE

The spatial distribution of protons perpendicular to the beam axis was measured to determine the region where primary reactions might have occurred in the bombarded target. The distribution at the target was estimated from multiple-scattering distribution approximations and was experimentally determined from measurements made with x-ray films and a beam profile counter telescope. The results were compared and the fraction of protons striking the target was estimated. For all spectral measurements,^{1,2} the size and shape of the beam were essentially the same, and the results of calculations for estimating proton losses are applicable in all experiments.

1. Neutron Phys. Div. Ann. Progr. Rept. Aug. 1, 1963, ORNL-3499, Vol. II.

2. Neutron Phys. Div. Space Radiation Shielding Research Ann. Progr. Rept. Aug. 31, 1962, ORNL CF-62-10-29 (Rev.), pp. 182-263.

UNCLASSIFIED
ORNL-DWG 64-7396

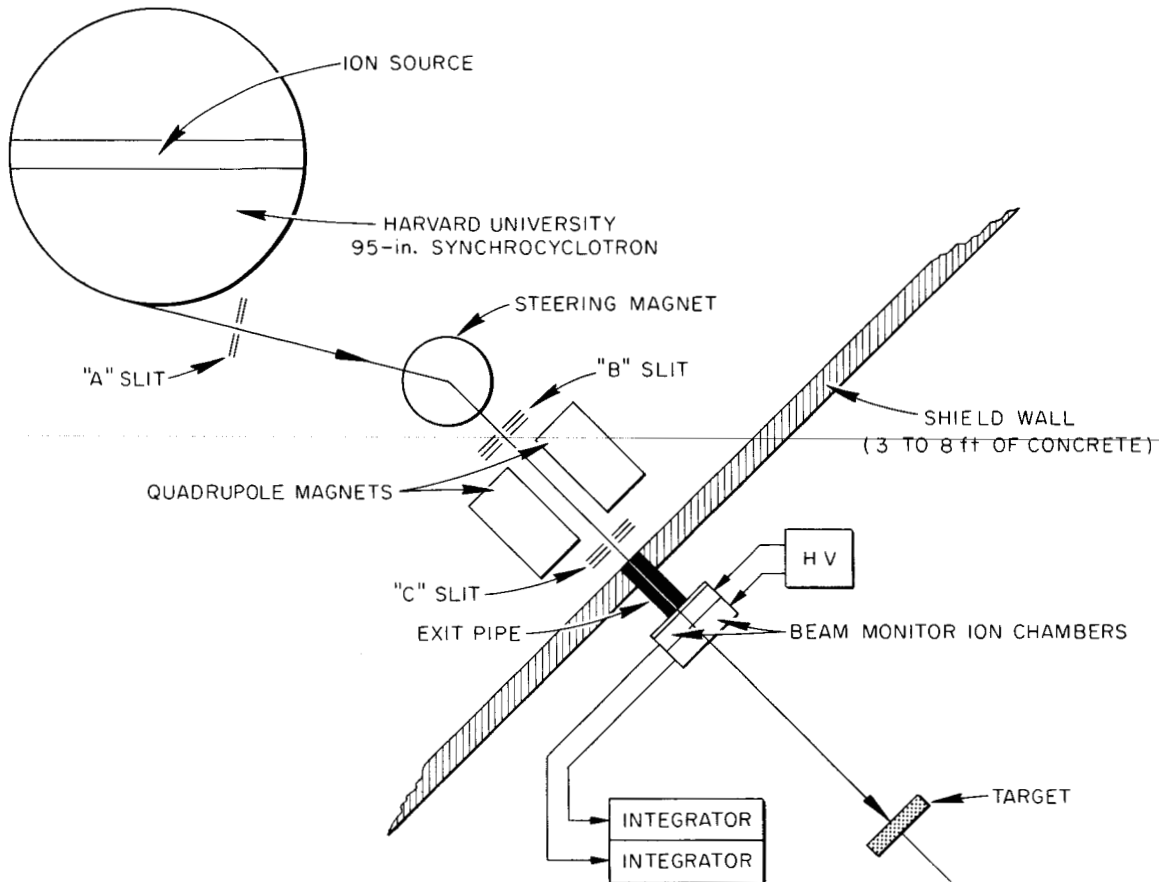


Fig. 1. Component Diagram of the Harvard University Synchrocyclotron.

Calculation of the Proton Distribution

When charged particles pass through materials of finite thickness, they undergo large numbers of electromagnetic collisions. The sequence of multiple collisions is characterized by numerous randomly oriented small-angle deflections, together with a smaller fraction of large-angle single-scattering deflections.

The scattering of these particles may be represented by the root-mean-square angle of scattering θ_{rms} , and when the multiple scattering dominates, the rms angle is proportional to the square root of the thickness of the scatterer. The scattering gives rise to a spread of the beam perpendicular to the direction of motion. The distribution of protons after multiple scattering can be approximated by a Gaussian function given by

$$P(r) = (\pi r_0^2)^{-1} e^{-(r/r_0)^2}, \quad (1)$$

where $P(r)$ is the probability per unit area of finding a particle with rms displacement, r , from the beam axis:

$$r_0 = \theta_{\text{rms}} D, \quad (2)$$

with D being the distance from the scatterer to the point at which the distribution is measured. Equation (1) gives the first-order approximation to the multiple-scattering distribution.

Snyder and Scott,³ using Fourier transforms, obtained a general expression for the scattering density function including all orders of scattering. They give the results of their calculations in graphic form over a wide range of target thickness and scattering angle. Figure 2 compares the full Snyder-Scott results with the (Gaussian) multiple-scattering approximation. The notation used is that of Snyder and Scott: η is proportional to the projected scattering angle θ_y , and $q(s, \eta)$ is proportional to the probability density

3. H. S. Snyder and W. T. Scott, Phys. Rev. 76, 270 (1949).

UNCLASSIFIED
ORNL-DWG 64-7390

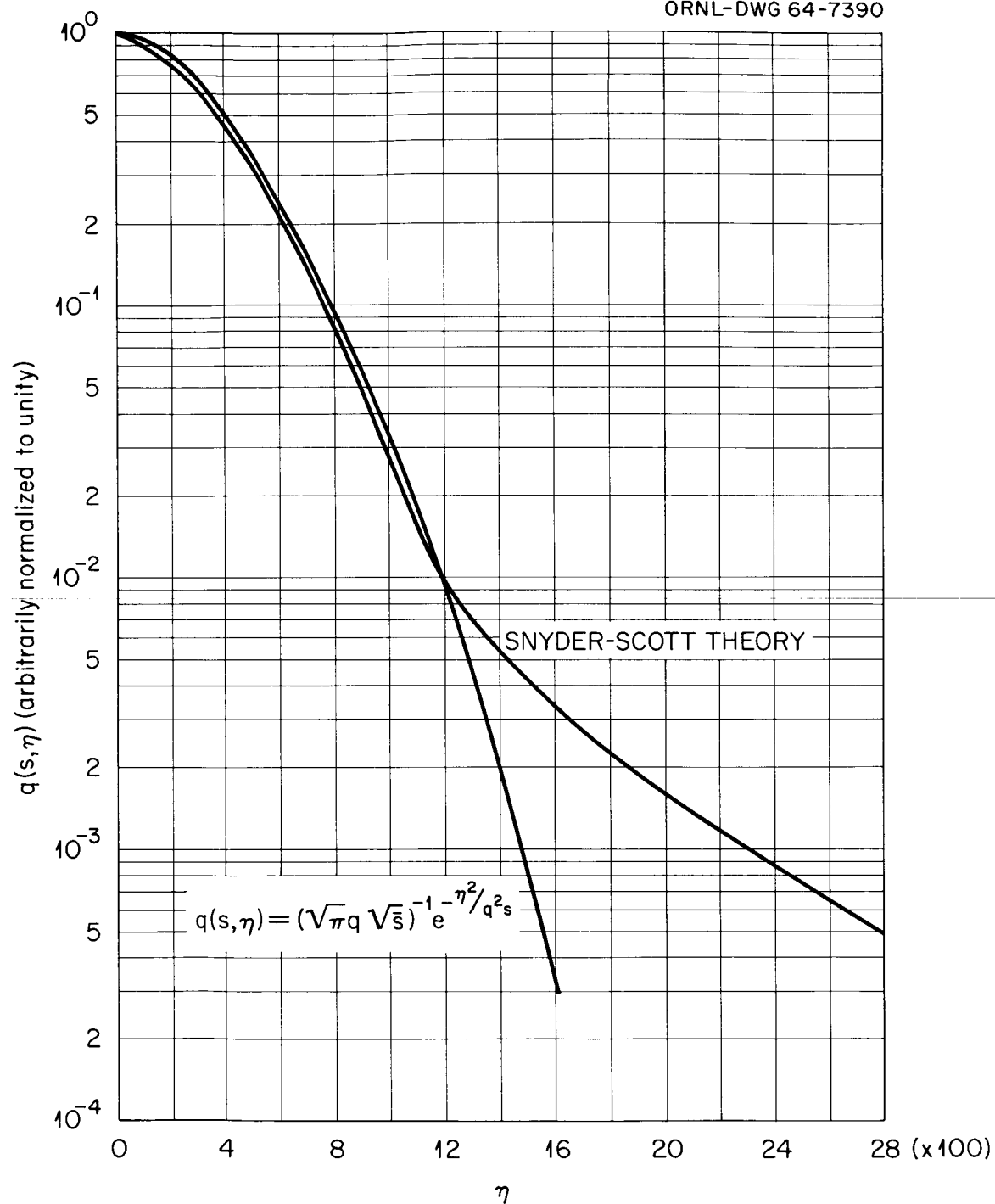


Fig. 2. Comparison of the Snyder-Scott Scattering Distribution with the Gaussian Approximation for $q(s, \eta)$ vs η with $q^2 = 15.4$, $\bar{s} = 21,000$.

function defining the fraction of protons in an angular interval $d\theta_y$ about θ_y . The scatterer parameters were chosen similar to those encountered in this experiment.

Plotting the results of Fig. 2 on a linear graph reveals that the ratio of the area between the Gaussian curve and the scattering tail to the area in the peak is negligible. The Gaussian multiple-scattering approximation gives sufficiently accurate results for estimating the scattering distribution at the target plane.

For this report, the scattering distribution at the target plane is obtained by using the Gaussian approximation only, and the fraction of protons at the target is calculated by the procedure suggested by Sternheimer.⁴

The rms angle of scatter of Eq. (2) is calculated from the expression

$$\theta_{\text{rms}}^2 = \left(\frac{E_s}{\beta c p} \right)^2 \sum_i \frac{x_i}{(X_s)_i}, \quad (3)$$

where E_s is a constant equal to 21 MeV, βc is the velocity of the incident particle, p is its momentum, $(X_s)_i$ is the multiple-scattering length in g/cm^2 of the i th scatterer material, and x_i is the thickness of the material in the beam. The scattering distribution is determined for the passage of the proton beam through the two monitor ionization chambers shown in Fig. 1. The combined scattering length of the chambers is obtained from the summation in Eq. (3). In passage through the chambers, the beam is scattered by 8 mils of aluminum, 2.5 mils of aluminized Mylar, and 5.0 cm of helium gas. Included is an additional 5-mil-thick Mylar beam pipe window. The scattering length of the combination of materials is equivalent to 0.078 g/cm^2 of aluminum, where $(X_s)_{\text{Al}} = 23.9 \text{ g/cm}^2$. This value is used in all subsequent calculations. Defining

$$\rho' = \rho_0/R$$

4. R. M. Sternheimer, Rev. Sci. Instr. 25 (11), 1070-1075 (1954).

and

$$r' = r_0/R ,$$

where ρ_0 is the rms radius of the assumed normally distributed unscattered beam, r_0 the rms scattering radius as in Eq. (2), and R the radius of the target; the fraction, f_p , of protons striking the target may be obtained directly from Sternheimer's curves. The value for ρ_0 , for this reporting, must be estimated since in the experiment no measurements were made of the unscattered beam radius. However, from photographs made at various points along the beam axis, reasonable estimates for the unscattered beam radius give $\rho_0 = 0.17$ cm. The results of these calculations are given in Table 1.

Experimental Results

The beam distribution was experimentally determined by exposing five x-ray film plates in a beam of nominally 4×10^6 protons/sec. The exposure, determined from the charge collected in the ionization chambers, was made over a range of $1.6 (+0.080) \times 10^7$ to $1.3 (+0.065) \times 10^9$ protons. The individual plates were developed simultaneously to ensure uniform transparency in the unexposed portions of the film. Initial analysis was achieved by measuring the fraction of light transmitted through the image by scanning with a photodensitometer. The slit openings of the densitometer were adjusted for a minimum opening of 10- μ width and 0.7-mm height. The scanning speed was 5 mm/min. The results of scanning the five plates are shown in Fig. 3. The profiles were aligned by defining the center of the full width at half maximum (FWHM) value of the transmission curves as the beam center line. From these data it was possible to construct the composite distribution curve shown in Fig. 4. This was done as follows.

1. The peak of the 1-nanocoulomb exposure curve, shown in Fig. 3 and defined as unit relative beam intensity, was plotted as point A on Fig. 4.
2. Following a line of constant transmission, shown by the dotted line in Fig. 3, the remaining transmission curves were intercepted at

TABLE 1. Comparison Between the Estimated Fraction of Protons, f_p , and Experimentally Measured Fraction of Protons, f_d , Striking the Target as a Function of the Target Radius R

R (cm)	$r' = \frac{r_o}{R}$ (a)	$\rho' = \frac{\rho_o}{R}$ (b)	f_p	f_d
3.8	0.083	0.044	1	1
0.84	0.376	0.202	0.98	0.98
0.56	0.564	0.304	0.94	0.86
0.28	1.120	0.607	0.35	0.39

^aBased on $r_o = 0.316$ cm, $D = 101.6$ cm, and $\theta_{rms} = 3.11 \times 10^{-3}$ radian.

^b $\rho_o = 0.17$ cm.

UNCLASSIFIED
2-01-058-886R1

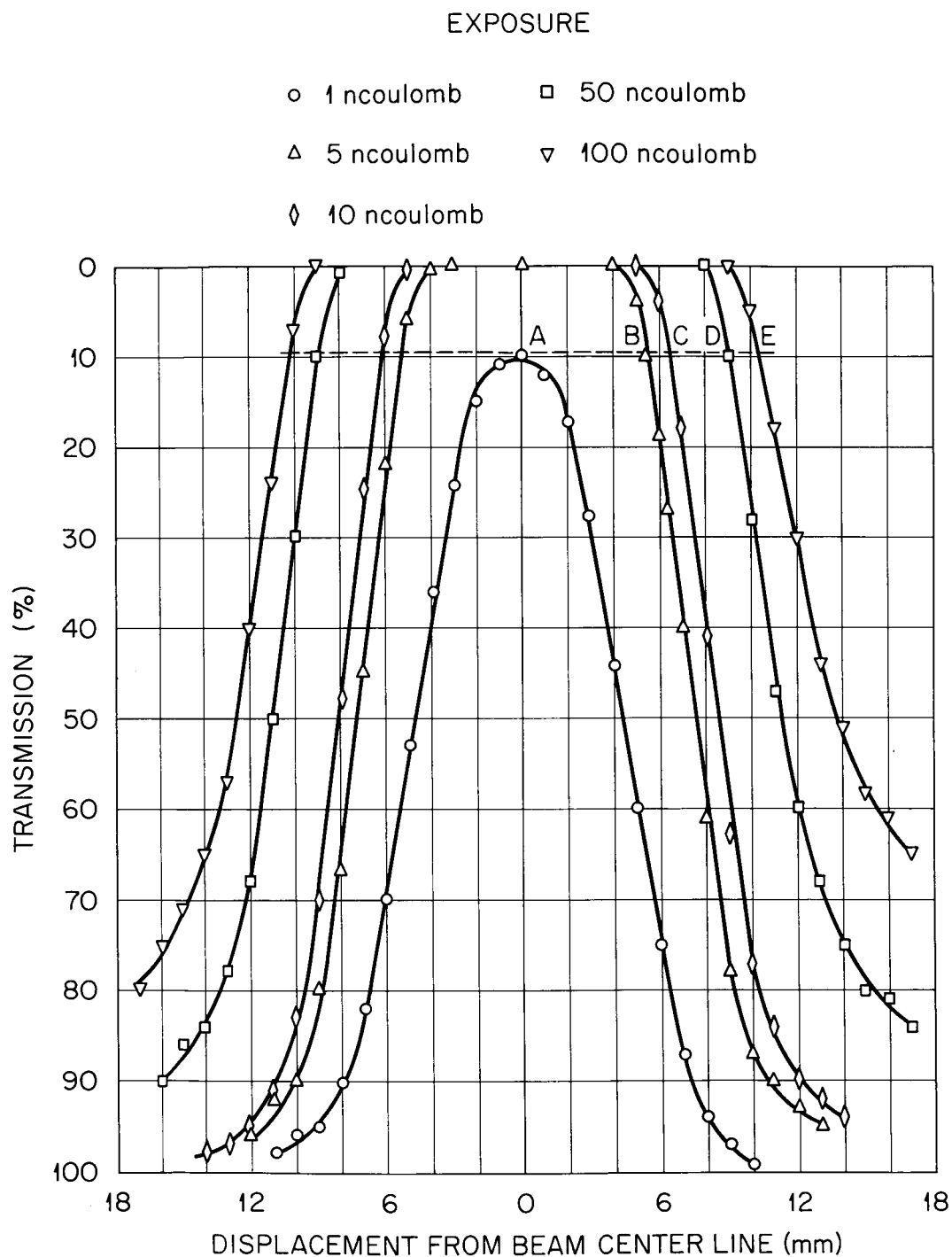


Fig. 3. Percent Transmission vs Image Width for Kodak Type-M Industrial X-Ray Film.

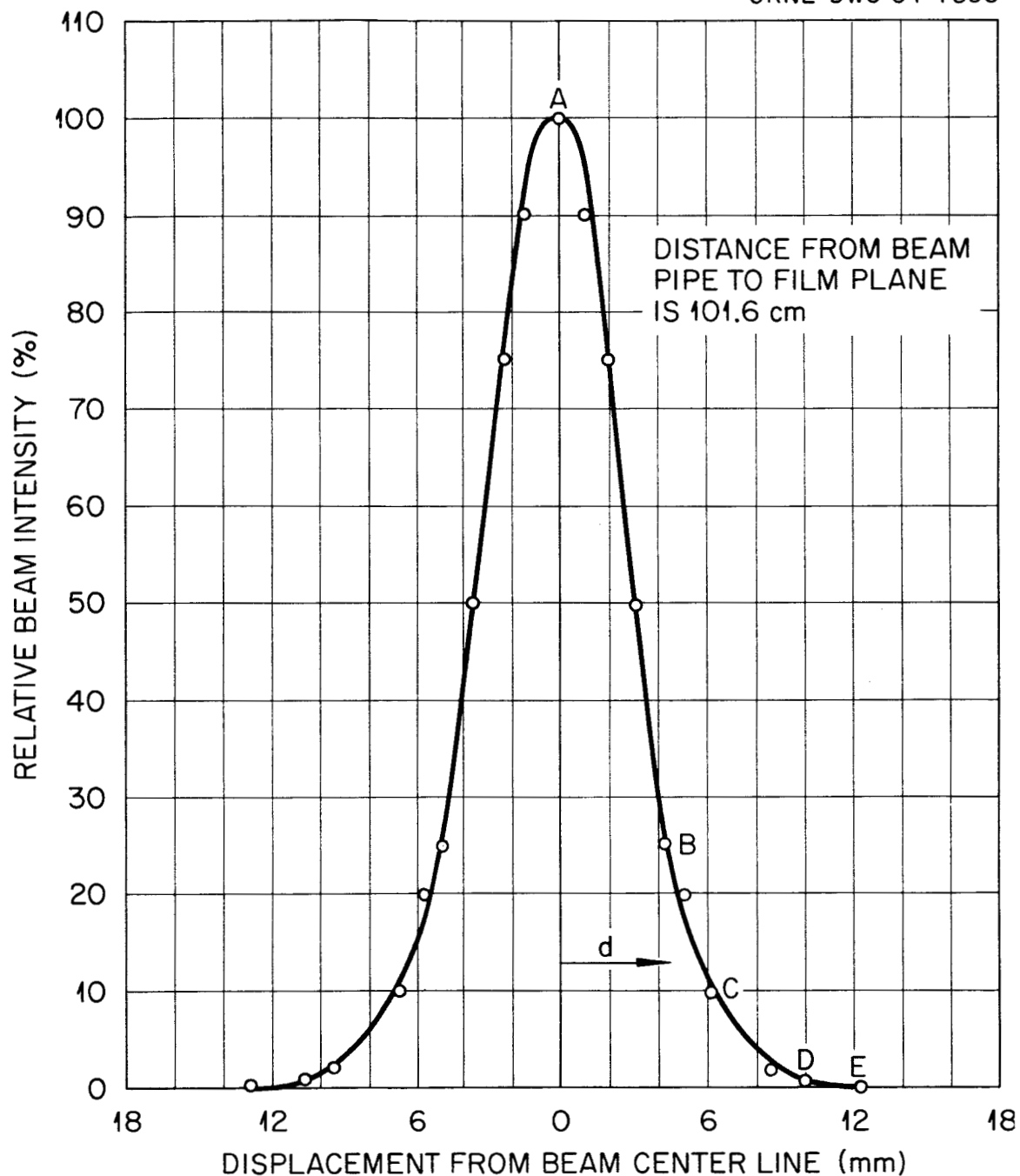
UNCLASSIFIED
ORNL-DWG 64-7395

Fig. 4. Composite Proton Distribution Curve. This curve is derived from Fig. 3 and plots the relative beam intensity as a function of beam diameter for Kodak Type-M industrial x-ray film.

points B, C, D, and E. Point B has the same width dimension as the 20% transmission level on the first curve, for example. The remaining points beyond these four were estimated from a calibration curve of the exposure-film density relationship obtained from the transmission curve data of Fig. 3.

The proton distribution was also measured with the profile telescope shown in Fig. 5. The distribution was obtained by scanning horizontally and vertically perpendicular to the beam axis and recording coincidence counts for fixed increments of integrated beam current as a function of displacement from the beam center at a distance of approximately 1 m from the ion chamber. The values obtained for FWHM for both the vertical and horizontal scan as well as other points on the distributions were in agreement, suggesting that the beam cross section was essentially circular. Figure 6 plots proton intensity as a function of the distance from the beam center line as obtained with the profile telescope.

The distribution curves in Figs. 4 and 6 are essentially Gaussian in shape. It was assumed from the exposures that the beam cross section was very nearly circular. If both conditions are true, the fraction of protons f_d contained within a radius d may be estimated from integration of a Gaussian frequency curve for the fitted value of $\langle d^2 \rangle^{1/2} = 0.28 \pm 0.01$ cm. Agreement between the x-ray film exposures and profile telescope data is excellent. Using the Gaussian frequency curve given above, integration of the curves in Figs. 4 and 6 gives the same results for f_d as shown in Table 1.

Beam Location Stability

Measurements of the time drift of the beam location with respect to the target center line were made with Polaroid film exposures in the target plane. Initially, the beam was centered on the target by proper location of the spectrometer holder and target positioning device. The location of the beam was checked several times during a particular experiment. It was observed that the beam drift was less than 5 mm/day with respect to the target center. Corrections for the drift were made by adjustment of the steering magnet.

UNCLASSIFIED
ORNL-DWG 64-7397R

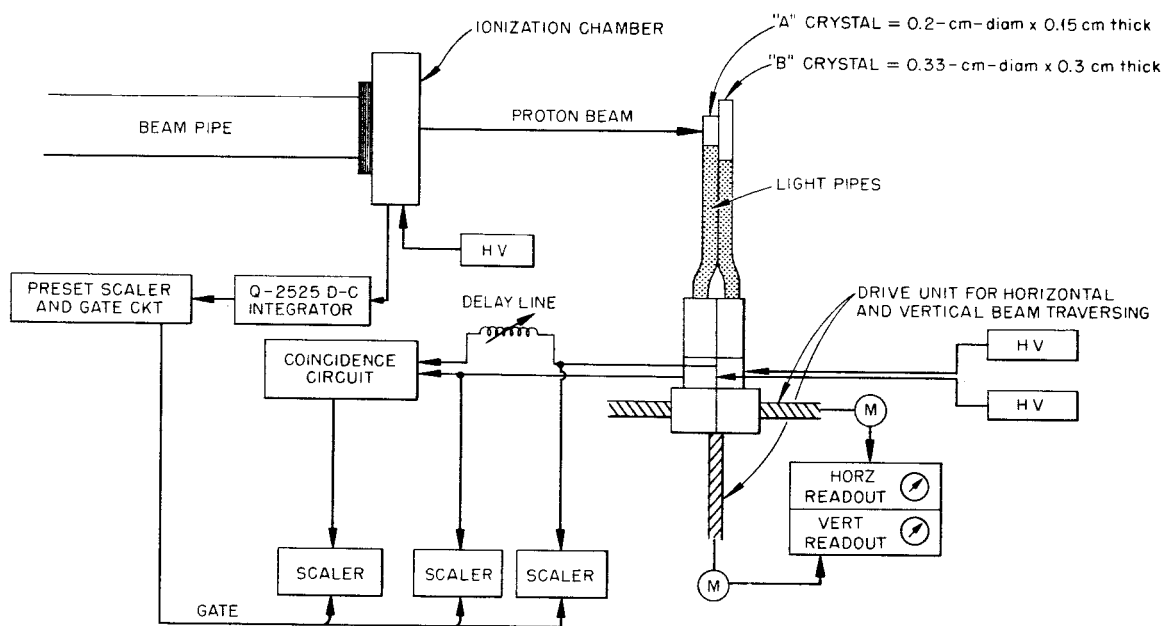


Fig. 5. Block Diagram of the Profile Telescope and Instrumentation.

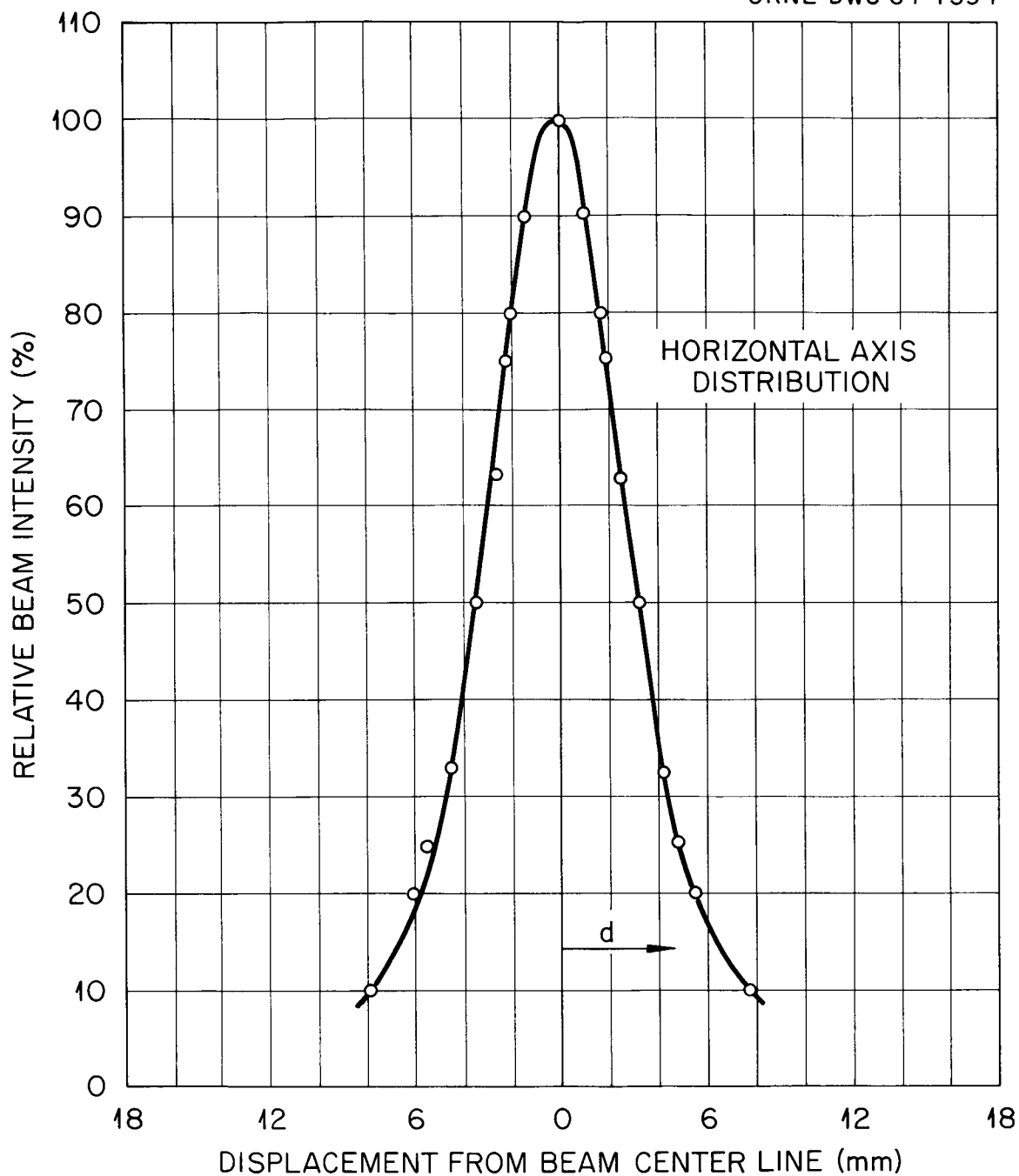
UNCLASSIFIED
ORNL-DWG 64-7394

Fig. 6. Proton Distribution Curve Obtained with the Profile Telescope. Relative beam intensity vs beam diameter. Distance from beam exit pipe equals 101.6.

DISTRIBUTION IN TIME

The distribution of the proton beam in time was determined from the measurement of the gross structure of the beam associated with the modulation frequency (macrostructure) and the fine time structure due to the r-f accelerating frequency (microstructure). In a synchrocyclotron the proton beam is extracted only when the frequency of the accelerating voltage is within a narrow range. In the Harvard synchrocyclotron, frequency modulation is achieved by a 16-tooth rotating capacitor operated at nominally 18 rps. Consequently, there are 288 bursts of protons per second. Because of variations in the shape of the capacitor teeth, wobble in its shaft, and variations in the rotation speed, the shape of the individual proton bursts varies in intensity and duration. In order to assess the effect of variation of the machine parameters on the gross duty cycle, the macroburst structure was studied as a function of ion source position and extraction frequency.

Measurement of the Macrostructure

The burst structure was measured with the circuit shown in Fig. 7. An organic detector was positioned in the beam. A marker pulse was available on the downswing of the FM cycle just before proton extraction; so the elapsed time between the marker pulse and a subsequent proton signal was analyzed and stored. The macrostructure was analyzed for the bursts associated with selected teeth of the rotating condenser and also for the composite structure. The duty factor was measured for the composite structure.

The gross duty factor can be obtained by measuring the ratio of the square of the average height of the burst to the average value of the height squared. The burst height is proportional to the output current from the detector used in Fig. 7. So the duty factor is obtained from

$$df = \frac{\langle \bar{I} \rangle^2}{\langle I^2 \rangle}, \quad (4)$$

where I is the time-dependent phototube current averaged over the rf (22 Mc) fine structure.

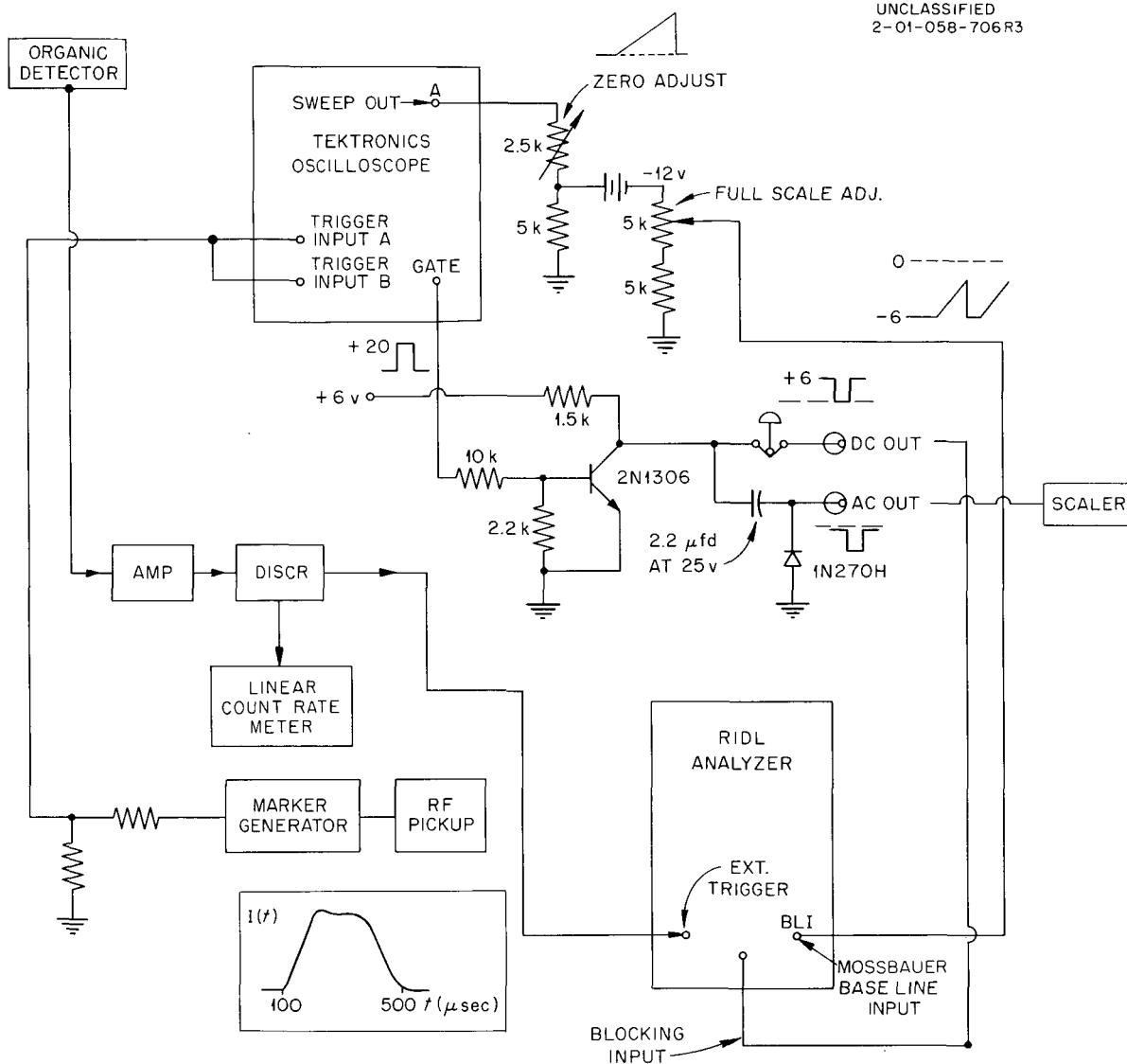
UNCLASSIFIED
2-01-058-706R3

Fig. 7. Circuit Used for Measuring the Beam Macrostructure. This circuit utilizes the Mossbauer base-line input provisions of the RIDL pulse-height analyzer. With this mode of operation, the analyzer associates a channel with the voltage of the negative pulse feeding this input at the time that the trigger pulse arrives from the proton detector. Zero volts corresponded to channel zero, and -6V was channel 100. With the oscilloscope sweep set at 50 μsec/cm and synchronized with the extraction-time marker pulse, an analyzer-enabling gate signal is generated each time the frequency passes through the extraction point. Thus a trigger pulse causes storage in a channel corresponding to the time that a proton appeared in a macroburst relative to the phase of the frequency modulation.

A typical composite burst shape is shown in the inset in Fig. 7. By approximating the burst by a triangle, rectangle, or both, the macroduty factor can be obtained quite readily by using this definition. Typical values obtained were $(4 \pm 2)\%$. The value obtained by Lefrancois⁵ using Eq. (4) to evaluate current from a phototube viewing a plastic scintillator was $(3 \pm 0.2)\%$. Zobel and Maienschein⁶ have reported values ranging from 2.4 to 4.9% by measuring random coincidence events during several runs. Values for the duty cycle of 2.2 to 4.55% were measured for a 5% variation in the extraction frequency, and 2.8 to 4.9% for variations in the ion source orientation at the extraction frequency of maximum duty factor.

In calculations that Peelle and Cowperthwaite⁷ made by using data from individual proton-counting measurements, the duty factor was measured as 2% for very low counting rates and narrow "B" slit openings (see Fig. 1).

Measurement of the Microstructure

A further study of the burst structure reveals a finer distribution of protons, called the "microstructure," with bursts occurring at the rf accelerating frequency. Knowledge of the microstructure was essential in the design of fast-timing circuits and gating circuits. The gating circuits were used to enable the detectors to operate only during the microbursts to minimize the accumulation of background counts due to secondary neutrons.

In measuring the microstructure an oscilloscope was used to observe individual proton pulses from a detector placed in the beam, together with the beam profile telescope, for which delayed coincidence techniques were used.

5. J. Lefrancois, Rev. Sci. Instr. 32, 986 (1951).

6. W. Zobel and F. C. Maienschein, private communication.

7. Neutron Phys. Div. Ann. Progr. Rept. Aug. 1, 1963, ORNL-3499, Vol. II, p. 73.

The pulses from an organic scintillator placed in the proton beam were used simultaneously to trigger an oscilloscope and provide the vertical input. The fine time structure was measured by observing on the cathode ray tube the relationship between the proton-induced trigger pulse and the pulse formation due to subsequent protons. The pulse frequency was constant, nominally 22.7 Mc/sec, with the width of the distribution of protons being less than 7 nsec. Observations made of the microstructure for many thousand pulses showed that the pulses occurred at regular intervals of ~ 42 nsec, and in no case was there any evidence of structure between the main pulses.

In the microstructure measurements with the profile telescope, the delay in one leg of the circuit was varied until coincidence was established between successive bursts. The amount of delay is the time between bursts. The telescope, initially set up to measure the beam profile, was located at one edge of the beam in order to count approximately 1 proton/sec. Typical resolution for coincidence varied from 3.5 to 6.2 nsec, depending on the coincidence circuit used. The required delay to establish coincidence between microbursts varied from 41.2 to 44 nsec, with the breadth of the peak varying from 4.5 to 6.3 nsec for the above resolving times. Typical results are shown in Fig. 8.

The time spectra of Fig. 8 can be approximated accurately by a Gaussian distribution, and its variance computed by the usual methods. The coincidence resolution curve is approximately trapezoidal in shape. The time distribution of pulses in adjacent microbursts can be calculated by taking the difference between the variance of the Gaussian and that of the trapezoidal distributions. The value obtained for the standard deviation of the time between pulses in adjacent bursts is 1.4 nsec.

PROTON ENERGY DISTRIBUTION

The energy distribution of the proton beam was determined from measurements of the proton range in copper and from flight-time measurements. These measurements were made in order to determine the energy of the beam after passage through the monitor ionization chambers shown in Fig. 1.

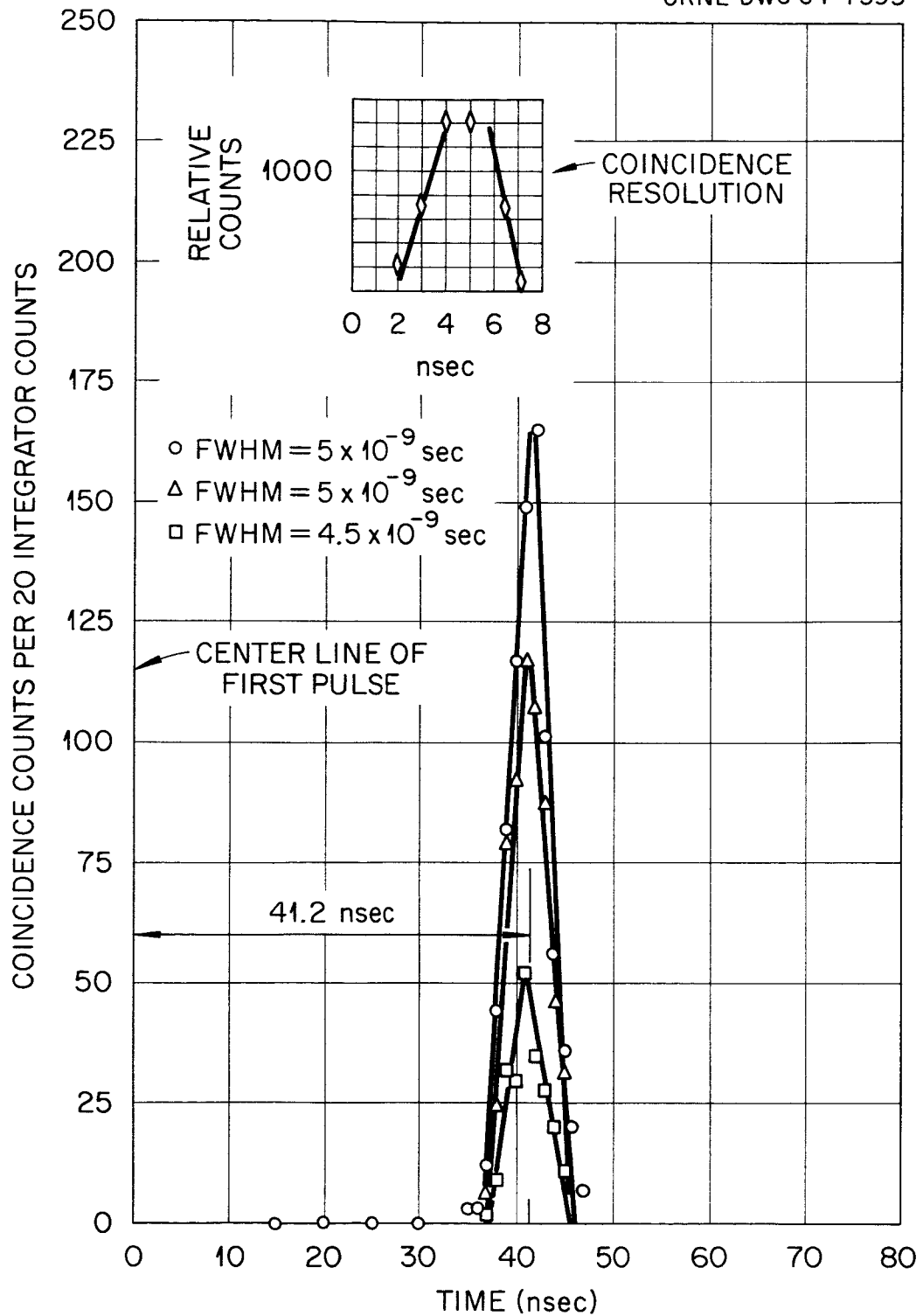
UNCLASSIFIED
ORNL-DWG 64-7393

Fig. 8. Measurement of Microstructure.

Beam Energy from Proton Range in Copper

Two independent measurements were made of the proton range in copper, one by Johnson⁸ (in September 1962) and the other by Santoro and Love (in January 1963), and different absorber blocks and detectors were used.

Two detectors were located in the beam path as shown in Fig. 9. The coincidence counts were recorded as a function of the thickness of the absorber placed between the two detectors for a fixed number of protons measured by the "A" detector, and are plotted in Fig. 10 for both measurements. The energy is determined from the curve by treating the maximum slope of the integral curve (the peak of the differential curve) as the mean range from protons of the incident energy in copper. This corresponds approximately to one-half the count rate with no absorber present.

The Range from Johnson's Measurements.-- The amount of copper present at the mean range was 26.326 g/cm^2 . Preceding the copper were 51.4 cm of air, 0.159 cm of CH, and 0.0051 cm of Al, corresponding to 0.062, 0.168, and 0.014 g/cm^2 surface density, respectively, for each material.

The ratio of $(dE/dx)_R$, the average energy loss per unit path length of a given material R, to $(dE/dx)_{Cu}$ is a slowly varying function of energy, and conversion to equivalent copper thickness depends only on approximate values for the incident energy. Using 160 MeV to evaluate these ratios, Johnson obtained a total copper-equivalent thickness of 0.348 g/cm^2 . Including an additional 0.011 g/cm^2 copper equivalent thickness for the small amount of air between the absorber and the "B" detector, the total amount of material in the beam was equivalent to 26.755 g/cm^2 of copper.

In these calculations, there were two main sources of error: the determination of the total copper thickness and the conversion between

8. C. F. Johnson, private communication. No information was available concerning B bias, which is here presumed to be very low. No uncertainty was given for determining the mean range from the experimental data.

UNCLASSIFIED
2-01-058-890A

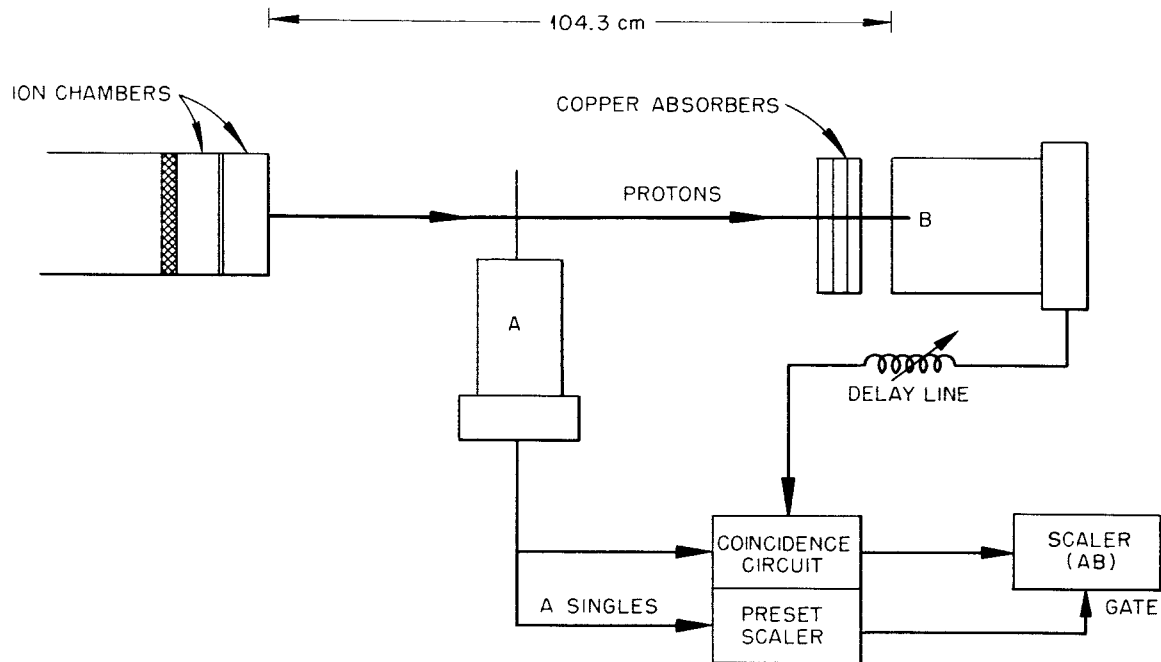


Fig. 9. Block Diagram of Circuit Used to Obtain Range-Energy Curve.

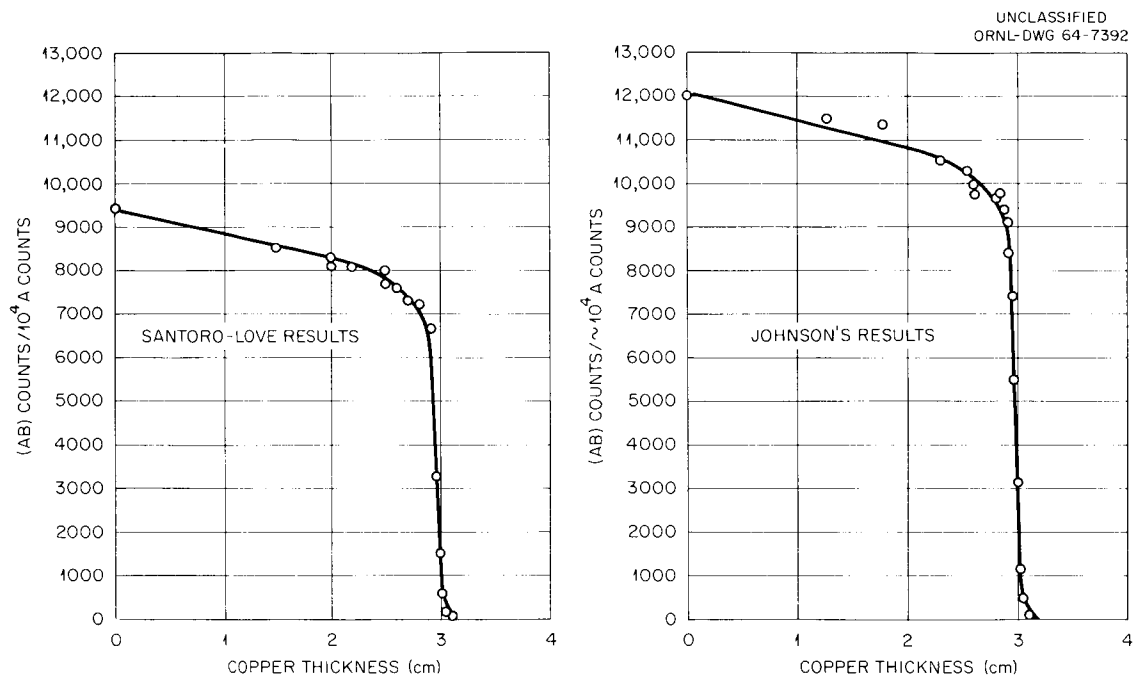


Fig. 10. Pathlength Energy Curves.

the mean range and energy. Measurements of the volume density of the copper introduced a $\pm 0.19\%$ error for one standard deviation based on measurements of the absorber dimensions and weight. Errors due to conversion to energy are discussed later. Then, finally, the mean range obtained by Johnson for the beam protons in copper is $26.755 \pm 0.051 \text{ g/cm}^2$.

Range Due to Santoro and Love. -- The second of the range-energy measurements was made with the apparatus shown in Fig. 9. The bias level of the "B" detector was set to count protons with energy in excess of $2 \pm 0.5 \text{ MeV}$. The bias was determined by using the 0.511- and 0.393-MeV gamma rays of ^{22}Na and ^{113}Sn , respectively. The uncertainty in the measurement of the energy resulting from the use of this bias setting was less than 0.1% , well within the other uncertainties.

The mean range of the protons was reached with $26.61 \pm 0.1 \text{ g/cm}^2$ of copper. Using a code due to Wachter,⁹ the additional material in the beam - the air, detector material, and aluminum detector covers - was calculated in terms of the equivalent thickness of copper as 0.376 g/cm^2 , giving a total of $26.98 \pm 0.1 \text{ g/cm}^2$ of copper.

The absorber plates were constructed to tolerances known to be better than 0.1% , and the weight was determined to the same order of magnitude. The volume density values for the air, aluminum, and detector materials were based on published values and since they constitute less than 2% of the material in the beam, only small errors were introduced in the conversion to equivalent copper thickness.

The value for the beam mean range in copper was then determined as $26.98 \pm 0.1 \text{ g/cm}^2$, which is consistent with the value obtained earlier by Johnson and is used in this report to determine the beam energy. This range must be corrected for the multiple scattering of the protons in copper. The correction value, 0.5% in range, was estimated from

9. J. W. Wachter, ESCALATOR, a program for the IBM-7090 which uses interpolation of range-tables to determine accumulative energy losses through various regions of materials (unpublished).

Bichsel's data for multiple scattering in nickel.¹⁰ The resulting experimental path length in copper is $27.11 \pm 0.1 \text{ g/cm}^2$.

Conversion of Path Length to Energy. -- The conversion of range to energy is based on published values for the path length of protons in copper, based on the average energy loss per g/cm^2 , dE/dx , obtained from the integration of the Bethe-Bloch equation

$$\frac{dE}{dx} = \frac{4\pi m_o^2 c^2 r_o^2 N_o}{\beta^2} \frac{z^2 Z}{A} \left(\ln \frac{2m_o c^2 \beta^2}{1 - \beta^2} - \beta^2 - \ln I - \frac{\sum C_i}{Z} \right), \quad (5)$$

where

x = path length, cm,

z = charge number of the incident particle,

Z = charge number of the stopping material,

A = atomic weight,

$\beta = v/c$, where v is the velocity of the particle and c is the speed of light,

N = Avogadro's number,

e = electronic charge,

m_o = rest mass of the electron,

I = average excitation potential per electron of stopping atom,

C_i = "shell-correction" term to compensate the effect of nonparticipating bound electrons.

According to the extent to which corrections are made for the C_i term and depending on the choice of experimentally determined values for I , values published for dE/dx may differ by a few percent.

For this report, Bichsel's¹⁰ values are used. These data are based on recently determined values for I and extensive corrections using the C_i terms. Additional credence has been given to Bichsel's

10. H. A. Bichsel, Passage of Charged Particles through Matter, American Institute of Physics, Handbook, 2nd Ed., McGraw Hill, 1963.

data in a more recent report by Fano.¹¹ Table 2 shows a comparison, over an energy range of 140 to 180 MeV, between Bichsel's values and those of Peelle,¹² Sternheimer,¹³ Rich and Madey,¹⁴ and Williamson and Boujot.¹⁵

Bichsel¹⁶ has noted a discrepancy between the calculated values for the mean range of protons in copper and those obtained experimentally. In the energy range between 70 to 110, at 150 and 190 MeV, experimental path lengths are 1.5% greater than Bichsel's best computed values. Accordingly, the values in Table 2 for the path length are corrected for the 1.5% difference, and the mean proton energy is computed. An uncertainty in the correction value of 0.5% is estimated.

The final calculated beam energy at the ionization chamber was 160.3 ± 0.6 MeV.

The range spread may be obtained by differentiating the range energy curve. The expected fluctuation in the path length of the protons is Gaussian with the ratio of the rms fluctuation, σ , to the total path length P given by

$$\frac{\sigma}{P} = \left[\sqrt{\frac{102.2}{Mc^2}} f\left(\frac{E}{Mc^2}\right) \right], \quad (6)$$

-
11. U. Fano, Ann. Rev. Nucl. Sci. 13, 1 (1963)
 12. R. W. Peelle, unpublished. These data use essentially the same parameters used by Bichsel.
 13. R. M. Sternheimer, Phys. Rev. 115(1), 137 (1959).
 14. M. Rich and R. Madey, Range-Energy Tables, UCRL-2301 (March 1954).
 15. C. Williamson and J. P. Boujot, Tables of Range and Rate of Energy Loss of Charged Particles of Energy 0.5 to 150 MeV, Report No. 2189, Centre d'Etudes Nucléaires de Saclay.
 16. H. A. Bichsel, Higher Shell Corrections in Stopping Power, Tech. Rept. No. 3, Department of Physics, University of Southern California, Los Angeles.

TABLE 2. Comparison of Published Values for the Path Length of Protons
in Copper and the Value for dE/dx

E (MeV)	Bischel		Peelle		Sternheimer		Rich and Medey		Williamson and Boujot	
	R (g/cm ²)	$\frac{dE}{dx}$ (MeV g ⁻¹ cm ⁻²)	R (g/cm ²)	$\frac{dE}{dx}$ (MeV g ⁻¹ cm ⁻²)	R (g/cm ²)	$\frac{dE}{dx}$ (MeV g ⁻¹ cm ⁻²)	R (g/cm ²)	$\frac{dE}{dx}$ (MeV g ⁻¹ cm ⁻²)	R (g/cm ²)	$\frac{dE}{dx}$ (MeV g ⁻¹ cm ⁻²)
140	21.171	3.847	21.124	3.856	21.63	3.767	~	~	21.648	3.753
150	23.83	3.673	23.779	3.682	24.34	~	23.85	3.661	24.412	3.59
160	26.614	3.519	26.555	3.528	27.19	3.445	~	~	~	~
170	29.513	3.383	29.447	3.391	~	~	~	~	~	~
180	32.524	3.261	32.452	3.268	33.23	2.192	~	~	~	~

ΔR (g/cm²) $\Delta \frac{dE}{dx}$ (MeV g⁻¹cm⁻²) ΔR (g/cm²) $\Delta \frac{dE}{dx}$ (MeV g⁻¹cm⁻²) ΔR (g/cm²) $\Delta \frac{dE}{dx}$ (MeV g⁻¹cm⁻²) ΔR (g/cm²) $\Delta \frac{dE}{dx}$ (MeV g⁻¹cm⁻²) ΔR (g/cm²) $\Delta \frac{dE}{dx}$ (MeV g⁻¹cm⁻²)

where Mc^2 is the rest mass energy of the proton in MeV, E is the kinetic energy of the proton, and $f(E/Mc^2)$ is obtained from Bichsel's¹⁰ work for range straggling.

For 160-MeV protons, $f(E/Mc^2) = 3.6\%$ and $\sigma = 0.32 \text{ g/cm}^2$ when P is 27 g/cm^2 as above. The measured straggling standard deviation obtained from the differential range-energy curve is $0.34 \pm 0.05 \text{ g/cm}^2$.

Measurement of the Proton Energy by Flight Time

The proton energy was also determined by measuring the flight time of the protons, with the apparatus shown in Fig. 11, over a distance of $355 \pm 1 \text{ cm}$. With the "A" and "B" detectors positioned about 75 cm apart, a calibration curve of stop delay vs analyzer channel number was obtained. The "B" detector was then moved 355 cm farther away, and the experiment was repeated. The time required for the protons to travel 355 cm was obtained from the amount of change in the stop delay required to re-establish time coincidence. From these data, which are shown in Fig. 12, the time required for the protons to travel 355 cm was $23.26 \pm 0.1 \text{ nsec}$. The uncertainty, thought to come from the differential nonlinearity of the time-to-pulse-height converter, arises from consideration of several points along the curve in Fig. 12.

The error in the measurement of the flight path is 0.27%. A 1% standard error in the delay line calibration also exists, so that the total error in the measurement of the flight time is 1.1%. The proton velocity is then $15.26 \pm 0.17 \text{ cm/nsec}$. Correcting for the energy loss (1.38 MeV) of the protons in the "A" detector and air, the beam energy determined by flight time is $153.38 \pm 4.1 \text{ MeV}$.

Conclusions to the Proton Beam Measurements

The energy obtained from the range-energy measurement, $160.3 \pm 0.6 \text{ MeV}$, and that obtained from the time-of-flight measurement, $153.38 \pm 4.1 \text{ MeV}$, are in mild disagreement. Both values, however, are in agreement with published¹⁷ values for the beam energy of $158 \pm 2 \text{ MeV}$.

17. F. T. Howard, Cyclotrons and High Energy Machines, ORNL-2644 (1958).

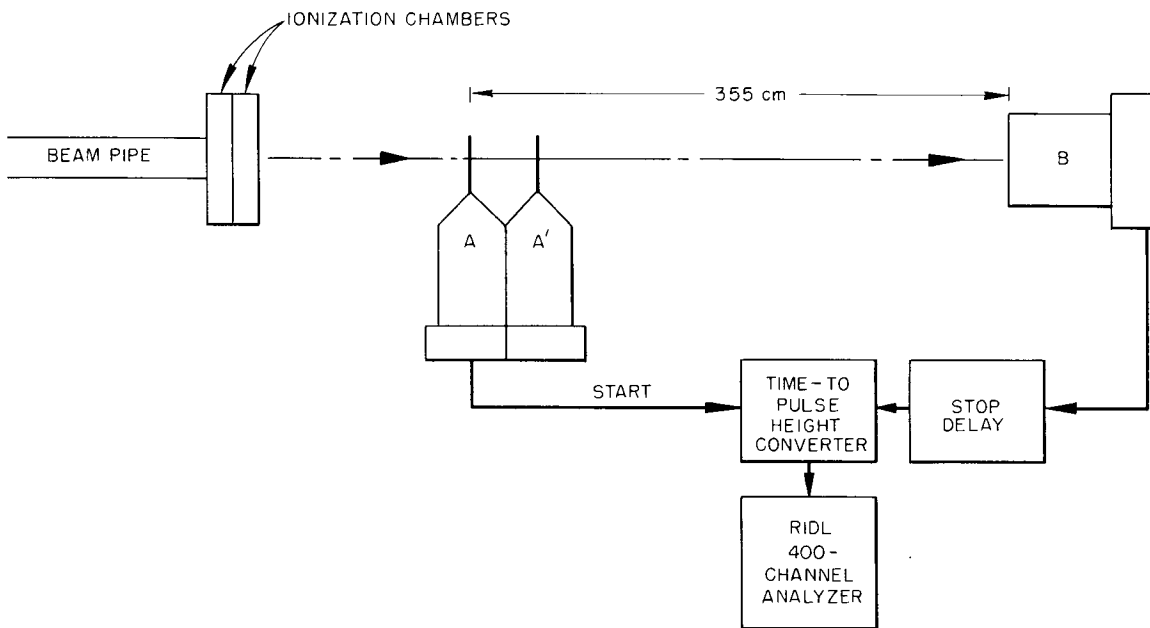
UNCLASSIFIED
2-01-058-892 A

Fig. 11. Block Diagram of Components for Proton Time-of-Flight Measurements.

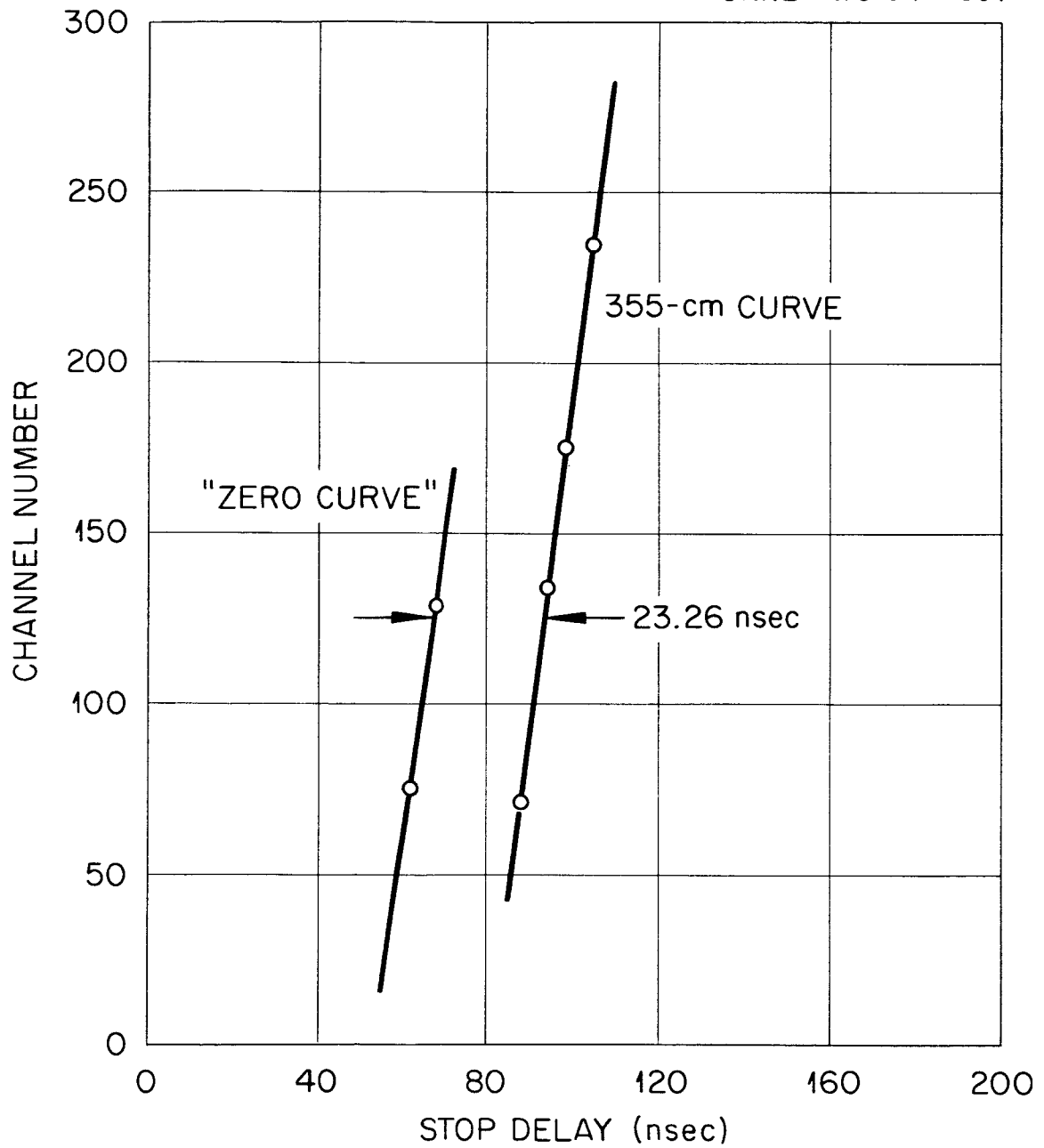
UNCLASSIFIED
ORNL-DWG 64-7391

Fig. 12. Flight-Time Curves for Measuring Proton Beam Energy.

ACKNOWLEDGMENTS

The author wishes to thank Harvard University and the Department of the Navy for the use of the synchrocyclotron and in particular Andreas Koehler of the University staff for his comments and advice concerning these measurements.

The efforts of R. W. Peelle in reviewing the drafts of this report are gratefully acknowledged.

Finally, the author acknowledges the work of E. Beckham, O. W. Christian, D. J. Kirby, F. E. Richardson, and H. Weaver for assistance in making the measurements. The efforts of C. O. McNew and R. A. Francis are also appreciated.

ORNL-3722
UC-34 - Physics
TID-4500 (36th ed.)

INTERNAL DISTRIBUTION

- | | |
|-------------------------------------|-----------------------------------|
| 1. Biology Library | 66. C. E. Larson |
| 2-4. Central Research Library | 67. H. G. MacPherson |
| 5. Reactor Division Library | 68. Robert Peelle |
| 6-7. ORNL - Y-12 Technical Library | 69. J. J. Pinajian |
| Document Reference Section | 70-84. R. T. Santoro |
| 8-57. Laboratory Records Department | 85. M. J. Skinner |
| 58. Laboratory Records, ORNL R.C. | 86. G. E. Stapleton |
| 59. R. Bender | 87. J. W. Wachter |
| 60. E. P. Blizard | 88. A. M. Weinberg |
| 61. Leroy Blumberg | 89. W. H. White, Jr. |
| 62. J. K. Dickens | 90. W. Zobel |
| 63. W. A. Gibson | 91. G. Dessauer (consultant) |
| 64. F. T. Howard | 92. M. L. Goldberger (consultant) |
| 65. W. H. Jordan | 93. R. F. Taschek (consultant) |

EXTERNAL DISTRIBUTION

- 94-96. NASA, Lewis Research Center, Cleveland, Ohio 44135 (1 copy each to Irving Karp, R. I. Hildebrand, and G. V. Brown)
- 97-99. Jet Propulsion Laboratory, Pasadena, California 31103 (1 copy each to D. F. Spencer, R. V. Meghreblan, and Robert Mackin)
- 100. M. J. Berger, Radiation Theory Branch, National Bureau of Standards, Washington, D.C. 20234
- 101. William Kreger, U.S. Naval Radiological Defense Laboratory, San Francisco, California 94135
- 102. Ludwig Katz, Air Force Cambridge Research Center, L. G. Hanscom Field, Massachusetts
- 103. H. J. Schaefer, U.S. Naval School of Aviation Medicine, Pensacola, Florida 32512
- 104. Sol Krasner, Office of Naval Research, Washington, D.C.
- 105. Lt. Duane Adams, Air Force Weapons Laboratory, WLRB-1, Kirtland Air Force Base, New Mexico
- 106. Lt. Col. Edward Harney, Air Force Space Systems Division, SSTA, Air Force Unit Post Office, Los Angeles 45, California
- 107. Lt. Col. J. R. Bohannon, Air Force Institute of Technology, NETF, Wright-Patterson Air Force Base, Ohio
- 108. Lt. V. H. Bouquet, Space Systems Division, SSTDS, Los Angeles 45, California
- 109. Lt. Col. C. D. Daniel, Jr., Defense Atomic Support Agency, Pentagon, Washington, D.C.
- 110. Lt. N. S. DeMuth, Jr., Air Force Weapons Laboratory, WLDN-2, Kirtland Air Force Base, New Mexico
- 111. H. J. Donnert, U.S. Army Nuclear Defense Laboratory, AMXND-C, Edgewood Arsenal, Maryland
- 112. Capt. R. E. Herman, Air Force Weapons Laboratory, SLRPH, Kirtland Air Force Base, New Mexico

- 113. Major Russell E. Linkous, Air Force Systems Command, SCTR,
Andrews Air Force Base, Maryland
- 114. T. J. McGuire, Systems Engineering Group, SESSV, Wright-
Patterson Air Force Base, Ohio
- 115. Major R. F. Mitchell, Air Force Systems Command, SCLDS,
Andrews Air Force Base, Maryland
- 116. L. H. Pittman, 6570th Aerospace Medical Research Laboratory,
Wright-Patterson Air Force Base, Ohio
- 117. Lt. Col. A. G. Swan, Aerospace Medical Division, AMRL, Brooks
Air Force Base, Texas
- 118. Ronald White, Air Force Flight Dynamics Laboratory, FDFE,
Wright-Patterson Air Force Base, Ohio
- 119-121. Aerospace Corporation, 2400 El Segundo Blvd., El Segundo,
California (1 copy each to F. L. Keller, Stan Freden, and
Robert Pruet)
- 122-124. North American Aviation, Inc., 12214 S. Lakewood Blvd., Downey,
California (1 copy each to Fred Raymes, E. R. Beever, and
J. D. Fletcher)
- 125-126. General Atomic, P. O. Box 608, San Diego, California (1 copy
each to Clyde Jupiter and George Joanou)
- 127-129. Boeing Airplane Company, Aerospace Division, P. O. Box 3707,
Seattle, Washington (1 copy each to Glenn Keister, Maynard
Pearson, and Brian Mar)
- 130-133. General Dynamics/Fort Worth, P. O. Box 748, Fort Worth, Texas
(1 copy each to E. C. Kidd and R. A. Miller, and 2 copies to
C. F. Johnson)
- 134-135. United Nuclear Corporation, 5 New Street, White Plains, New
York (1 copy each to Richard Ross and Phil Mittleman)
- 136. C. Zerby, Union Carbide Research Institute, P. O. Box 278,
Tarrytown, New York
- 137. Jim Johnson, Ling-Temco-Vought Research Center, P. O. Box 5003,
Dallas, Texas
- 138. C. W. Hill, Lockheed-Georgia Company, Marietta, Georgia
- 139. Ed Kuhn, Republic Aviation Corporation, Power Conversion
Systems Division, Farmingdale, L.I., New York
- 140. Keith More, Bendix Systems Division, 3300 Plymouth Road, Ann
Arbor, Michigan
- 141. Robert Siegel, College of William and Mary, Department of
Physics, Williamsburg, Virginia
- 142. John W. Freeman, Rice University, Houston, Texas
- 143. R. A. Glass, Lockheed Missiles and Space Company, 3251 Hanover
Street, San Jose, California
- 144. Tino Ahrens, Advanced Research Corporation, 715 Miami Circle,
N.E., Atlanta, Georgia
- 145-146. Radiation Research Associates, 1314 Hurley Avenue, Fort Worth,
Texas (1 copy each to R. L. French and Norman Schaeffer)
- 147. Sam V. Nablo, Ion Physics Corporation, Burlington, Massachusetts
- 148. R. C. Good, Jr., General Electric Company, P. O. Box 8555,
Philadelphia, Pennsylvania
- 149-150. Northrop Space Laboratories, Hawthorne, California (1 copy
each to R. E. Fortney and M. C. Chapman)
- 151. Sidney Russak, The Martin Company, Baltimore, Maryland

- 152-154. University of California, Lawrence Radiation Laboratory,
Berkeley, California 94720 (1 copy each to Cornelius Tobias,
Roger Wallace, and Charles Sondhaus)
- 155-156. Bellcomm, Inc., 1100 17th Street, N.W., Washington, D.C., 20036
(1 copy each to Tim Orrok and E. N. Shipley)
- 157. E. M. Finkelman, Grumman Aircraft Engineering Corporation,
Bethpage, Long Island, New York
- 158-159. McDonnell Aircraft Corporation, P. O. Box 516, St. Louis,
Missouri 63166 (1 copy each to R. L. Kloster and R. V.
Glowszowski)
- 160-162. General Dynamics/Astronautics, P. O. Box 166, San Diego,
California 92112 (1 copy each to D. H. Robey, A. W. McReynolds,
and E. L. Noon)
- 163-164. Westinghouse Electric Company, Research and Development Center,
Pittsburgh, Pennsylvania (1 copy each to D. W. Drawbaugh and
S. H. Autler)
- 165. R. L. Seale, University of Arizona, Tuscon, Arizona
- 166. R. G. Riedesel, Douglas Aircraft Company, Missile and Space
Division, Santa Monica, California
- 167. Borje Larsson, University of Uppsala, The Gustaf Werner
Institute, Uppsala, Sweden
- 168. R. D. Evans, Professor of Physics, Massachusetts Institute of
Technology, Cambridge, Massachusetts
- 169. S. P. Shen, Guggenheim Aerospace Laboratories, New York
University, University Heights, New York, New York
- 170. NASA Representative, Scientific and Technical Information
Facility, P. O. Box 5700, Bethesda, Maryland
- 171. Lt. Col. R. G. Allen, Jr., USAF Aerospace Medical Center,
Brooks Air Force Base, Texas
- 172. C. K. Bauer, Department 72-34, Z-26, Lockheed-Georgia Company,
Marietta, Georgia
- 173. N. Barr, Chief, Radiological Physics Branch, Division of
Biology and Medicine, U.S. Atomic Energy Commission,
Washington, D.C.
- 174. S. Bresticker, Grumman Aircraft Engineering Corporation, Space
Sciences Group, Plant 5, Bethpage, Long Island, New York
- 175. T. H. Colvin, Nuclear Sciences and Space Power Department,
Bendix Systems Division, 3300 Plymouth Road, Ann Arbor,
Michigan
- 176. Col. J. Conner, Biotechnology and Human Research, Office of
Advance Research and Technology, National Aeronautics and
Space Administration, Washington, D.C.
- 177. Capt. R. F. Cooper, ASRPE-20, Wright-Patterson Air Force Base,
Ohio
- 178. R. B. Curtis, University of Indiana, Bloomington, Indiana
- 179. C. A. Dempsey, 6570 AMRL, Wright-Patterson Air Force Base, Ohio
- 180. T. W. De Vries, General Dynamics, Fort Worth, Texas
- 181. Ed Divita, 1504 Doxbury Road, Towson, Maryland
- 182. D. L. Dye, Boeing Aircraft Company, Seattle, Washington
- 183. F. Felberg, Jet Propulsion Laboratory, Pasadena, California
- 184. K. D. George, Reactor Requirement Office, Building 407,
Pictinny Arsenal, Dover, New Jersey

185. R. L. Harvey, Room 173, Building A, General Electric Company, 175 Curtner Avenue, San Jose, California
186. J. F. Kenney, Boeing Scientific Research Laboratories, Post Office Box 3981, Seattle, Washington
187. M. R. Kinsler, North American Aviation, Inc., Space and Information Systems Division, 12214 Lakewood Blvd., Downey, California
188. David Langford, Pratt and Whitney Aircraft, East Hartford, Connecticut
189. W. H. Langham, Los Alamos Scientific Laboratory, Los Alamos, New Mexico 87544
190. L. R. Lewis, Nuclear Sciences and Space Power Department, Bendix Systems Division, 3300 Plymouth Road, Ann Arbor, Michigan
191. Martin Leimdorfer, Research Institute of National Defense, FOA4, Stockholm 80, Sweden
192. S. H. Levine, Northrop Space Laboratories, 3401 W. Broadway, 452/66, Hawthorne, California
- 193-217. Winnie M. Morgan, Technical Reports Office, Grants and Research Contracts, Office of Space Sciences, National Aeronautics and Space Administration, Washington, D.C. 20546
218. L. W. McCleary, Space and Information Systems Division, North American Aviation, Inc., Downey, California
219. J. C. Noyes, Boeing Scientific Research Laboratories, Box 3981, Seattle, Washington
220. J. P. Neissel, General Engineering Laboratory, General Electric Company, Schenectady, New York
221. Wade Patterson, University of California, Lawrence Radiation Laboratory, Berkeley, California
222. Col. J. E. Pickering, USAF Aerospace Medical Center, Brooks Air Force Base, Texas
223. Evalyn Repplinger, Crew Systems Division, P. O. Box 1537, Houston, Texas
- 224-228. O. Reynolds, Director, Bio-Science Programs, Office of Space Sciences, National Aeronautics and Space Administration, Washington, D.C.
229. General C. Roadman, Director, Aerospace Medicine Division, Office of Manned Space Flight, National Aeronautics and Space Administration, Washington, D.C.
230. T. J. Rock, General Dynamics/Fort Worth, Fort Worth, Texas
231. H. J. Schulte, Bellcomm, Inc., 1100 17th Street, N.W., Washington, D.C.
232. W. M. Schofield, Advanced Research Corporation, 3127 Maple Drive, Atlanta, Georgia
233. G. D. Smith, Ames Research Center, Moffett Field, California
234. Jerry Speakman, 6570 AMRL (MRBBR), Wright-Patterson Air Force Base, Ohio
235. R. H. Steelle, NASA, Manned Spacecraft Center, Houston, Texas
236. T. R. Strayhorn, S-71, General Dynamics, Fort Worth, Texas
237. William Steigelmann, Kuljian Corporation, 1200 North Broad Street, Philadelphia, Pennsylvania
238. F. C. Schwenk, NASA, Code NPO, Washington, D.C. 20546

- 239. M. A. Van Dilla, Los Alamos Scientific Laboratory, P. O. Box 1663, Los Alamos, New Mexico
- 240. Frank Voorhis, USAF (MC), OART/RBH, NASA, Washington, D.C.
- 241. F. Voris, Biotechnology and Human Research, National Aeronautics and Space Administration, Washington, D.C.
- 242. G. P. Wachtell, Franklin Institute, 20th and Parkway, Philadelphia, Pennsylvania
- 243. G. T. Western, S-71, General Dynamics/Fort Worth, Fort Worth, Texas
- 244. G. A. Whan, Associate Professor, Nuclear Engineering Laboratory, The University of New Mexico, Albuquerque, New Mexico
- 245. Maurice Wilkinson, The Boeing Company, M. S. 21-31, Seattle, Washington
- 246. K. Ziock, Department of Physics, University of Virginia, Charlottesville, Virginia
- 247. Marcello Zocchi, Reactor and Radiations Division, National Bureau of Standards, Washington, D.C.
- 248. Pierre LaFore, Commissariat a L'Energie Atomique, Centre D'Etudes Nucleaires, de Fontenay-aux-Roses (Seine), Boite Postale No. 6, France
- 249. A. M. Sarius, Centro Di Calcolo, CNEN, Via Mazzini 2, Bologna, Italy
- 250. A. M. Koehler, Physics Department, Harvard University, Cambridge, Massachusetts
- 251. H. A. Bichsel, University of Southern California, Los Angeles
- 252. Research and Development Division, AEC, ORO
- 253. V. B. Bhanot, Physics Department, Panjab University, Chandigarh-3, India
- 254-898. Given distribution as shown in TID-4500 (36th ed.) under Physics category (75 copies - CFSTI)